Dynamic Phase Compensation in Modulated-Demodulated Control for Pulsed Jet Injection

Cory Hendrickson and Robert M'Closkey

Abstract— This paper proposes the addition of dynamic phase compensation to modulated-demodulated controllers used for disturbance rejection/reference tracking and demonstrates a novel application of repetitive control for pulsed jet injection. In cases where a plant has rapidly varying phase near the frequency or frequencies to be controlled, conventional static phase compensation may be inadequate due to the propensity to create peaking in the sensitivity function. Dynamic phase compensation improves the disturbance rejection characteristics of modulated-demodulated controllers by inverting the plant phase over some frequency band in the "baseband" coordinates. Both static and dynamic phase compensation controllers are compared on an experimental apparatus that is used to study pulsed jet injection. The controllers are used to track a square wave in the temporal velocity profile of a pulsed jet of air using active forcing. In this application pulsing the jet improves the mixing and spread of the jet which are useful for energy generation and aerospace applications.

I. INTRODUCTION

The ability to reject periodic disturbances or track periodic references is a common requirement in many engineering systems. As such, there has been extensive research on repetitive control documented in the literature over a wide range of applications such as industrial machinery [1], computer disk drives [2], [3] and helicopter blade control [4], [5]. The many different types of repetitive controllers are united in their basis, directly or indirectly, on Francis and Wonham's Internal Model Principle (IMP) [6] which requires a model of the disturbance or reference to be included in the feedback loop for perfect rejection or tracking. The most common type of repetitive controller is based on a time delay placed in the feedback loop. A basic time delay controller has the form

$$C_{td}(s) = \frac{e^{-Ls}}{1 - e^{-Ls}}$$

which uses a delay of period L. The controller places infinitely many poles on the imaginary axis at intervals equal to the period of the delay. Therefore, according to the IMP, perfect rejection or tracking of periodic signals at frequency $1/L$ and all its harmonics is possible. These controllers offer quick execution speed at a large number of frequencies but are restricted to controlling the harmonics of the fundamental time delay.

Another type of repetitive controller is based directly on the IMP by using an oscillator in the feedback loop. The controller has the form

$$C_{imp}(s) = \frac{ks}{s^2 + \omega_n^2}$$

which places marginally stable poles at $\pm j\omega_n$. Multiple modes are controlled by placing copies of C_{imp} with different resonant frequencies in parallel. This controller provides selective placement of the poles but becomes difficult to stabilize as more modes are required due to coupling between neighboring modes.

An alternative implementation of the IMP controller is modulated-demodulated control, sometimes referred to as adaptive feedforward control or adaptive feedforward cancellation [7], [8]. This approach shifts the spectrum of "high" frequency oscillations down to a baseband which includes DC, operates at the baseband, then shifts the baseband spectrum back to high frequency. Essentially, the plant output at the frequency to be controlled is estimated, then manipulated to form an input based on known plant dynamics which will cancel the estimated output or track a reference signal. These controllers offer the benefit of using low bandwidth compensators to control high frequency oscillations. The modulated-demodulated controller is based indirectly on the IMP as shown in [9], where Bodson et al. proves an equivalence between a simple modulated-demodulated controller and an IMP controller.

Most modulated-demodulated control studies to date have focused on disturbance rejection as in [10] and [11] where a modulated-demodulated controller is used for vibration damping in flexible structures. Their analysis shows an LTI transfer function for this controller can be derived from two different perspectives, either the high frequency control band or the low frequency baseband. The control band analysis provides information on performance while the baseband analysis provides insight into the controller design.

The present paper expands upon the insight gained from the baseband analysis of [10] and presents an improved method of phase compensation for modulated-demodulated control. Replacing conventional static phase compensation with dynamic phase compensation improves disturbance rejection nearby the specified rejection or tracking frequency. Additionally, static phase and dynamic phase modulated-demodulated controllers are used to demonstrate a novel application of repetitive control for pulsed jet injection. Actively pulsing a jet can influence important aspects of the flowfield such as the spread and mixing of the jet into its surroundings. It is hypothesized these parameters will be maximized with the formation of strong, well-spaced

vortex rings at the jet exit in response to periodic square wave forcing. Challenges are presented in forming square waves due to non-linear dynamics identified in our actuation system. Repetitive control is necessary to shape the jet's measured temporal velocity waveform to track, as closely as possible, a square wave.

II. EXPERIMENTAL SETUP

A. Actuation System

The modulated-demodulated controllers developed in this study are implemented using the experimental setup for pulsed jet injection presented in Figure 1. The jet fluid is provided by a compressed air source which is regulated to maintain an average jet velocity of $8 \ ms^{-1}$ measured using a hotwire anemometer placed at the exit of a contracting nozzle. The regulated air supply is injected into a plexiglass plenum, or mixing chamber, beneath the nozzle. Active forcing is applied using a lightweight piston located approximately 14cm beneath the hotwire at the bottom of the sealed plenum. The piston is rigidly connected to an electromechanical shaker, which moves the piston axially in line with the jet using a large voice coil. The controllers are digitally implemented using Matlab's XPC Target application. The sampling rate is 25kHz. Anti-alias filtering of the hotwire signal is accomplished using an 8 pole Chebyshev filter with a 10kHz corner frequency.
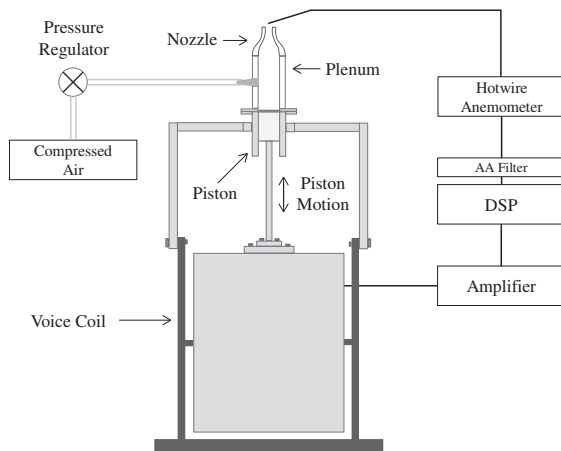

Fig. 1. Pulsed jet injection experimental setup using a piston to actively control the temporal velocity waveform of a jet at the nozzle exit.

B. System Identification

The piston actuation system was identified from 10Hz to 5kHz using a band-limited white noise input whose intensity is adjusted so the RMS velocity perturbation is $0.2 \ ms^{-1}$. As shown in Figure 2, the frequency response rolls off after a plenum mode near 2kHz, beyond which the jet velocity is nearly impossible to perturb. Due to the discontinuity in the waveform, the Fourier series coefficients of a square wave decay at a slow rate as a function of frequency. Thus, given the limited actuation bandwidth, only a truncated version of an ideal square wave can be formed using a limited number

of harmonics of the fundamental forcing frequency. It is important to use as many harmonics as possible to minimize deviations from the ideal square wave velocity profile.

In addition to the roll-off, another important aspect of the frequency response is a large amount of phase delay over the frequency band of interest. The phase delay is a result of the transport lag caused by the physical distance between the actuator and sensor (piston and hotwire). Such a large phase delay makes high-gain, wideband control impossible across the entire usable bandwidth of the actuator. Thus, instead of using a wideband approach, our control problem will be broken down into multiple narrow-band control problems using modulated-demodulated control, with each frequency band positioned around the fundamental frequency and harmonics of the periodic reference waveform.
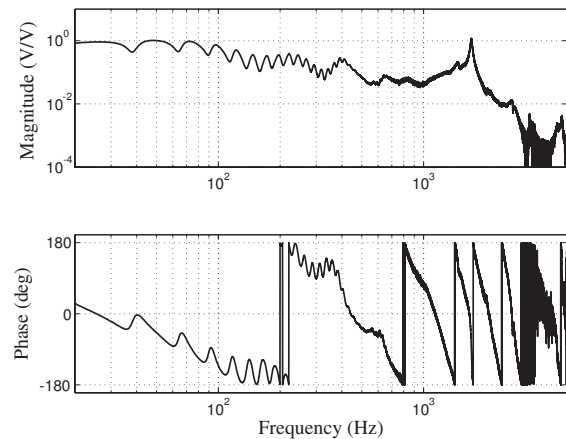

Fig. 2. Actuation system frequency response. Significant transport lag makes high gain, wide bandwidth control impossible to achieve.

III. CONTROLLER ARCHITECTURE

The controller uses feedback from a hotwire anemometer placed at the jet exit. A parallel set of individual control loops is used, each designed to operate in the neighborhood of a single frequency with the overall goal of tracking a desired periodic waveform. Due to the periodic nature of forcing, the operating frequencies are positioned at a fundamental forcing frequency, denoted ω_f, and all harmonics that fall within the actuation system's bandwidth. Thus, the ideal waveform will match the Fourier series approximation of the desired waveform truncated at the actuation system bandwidth. In practice, the Fourier series of the reference square wave are adjusted to compensate for the anti-aliasing filter lag.

A. Control at a Single Frequency

A diagram of the controller for regulation in a neighborhood of a single frequency, denoted ω_n, is shown in Figure 3. The output of the plant, $P(s)$, is split into two branches, an in-phase branch and a quadrature branch which are demodulated down to baseband by $2\cos(\omega_n t)$ and $2\sin(\omega_n t)$. Each branch then passes through identical low pass filters, $H_{LP}(s)$ with corner frequency ω_c. The response of y in a neighborhood of ω_n is captured by the near DC terms y_1 and y_2, i.e.
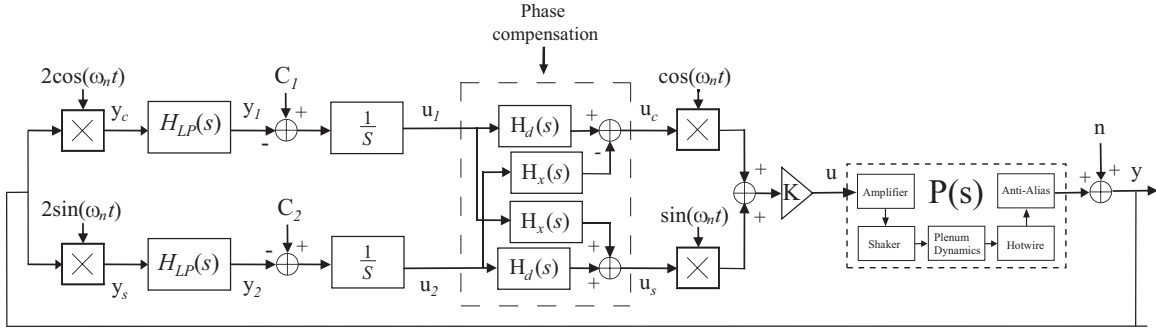
Fig. 3. Dynamic phase compensation modulated and demodulated controller for control at a single frequency

$$y(t) = y_1(t)\cos(\omega_n t) + y_2(t)\sin(\omega_n t)$$

The corner frequency of $H_{LP}(s)$ is limited as $\omega_c < \omega_f$ to eliminate interaction between controllers at adjacent harmonics.

The reference signals, represented by constants C_1 and C_2, are compared with y_1 and y_2 to produce error signals which are integrated for zero steady-state tracking error. References C_1 and C_2 represent the real and imaginary part of the Fourier series coefficient of a periodic reference waveform at frequency ω_n, i.e. the desired plant output has the form

$$y(t) = C_1 \cos(\omega_n t) + C_2 \sin(\omega_n t).$$

The integrated error signal passes into a phase compensation stage using either static or dynamic compensation which inverts the plant phase phase at, or around, ω_n. The phase-compensated signals are then modulated back to the control band by multiplication with $\cos(\omega_n t)$ and $\sin(\omega_n t)$. At this point, the split signals are summed and scaled by K to form the control effort u.

Phase compensation in modulated-demodulated control is needed for improved stability margin and to reduce the sensitivity function of the closed-loop system nearby ω_n. Using conventional static phase compensation, the compensators $H_d(s)$ and $H_x(s)$ in Figure 3 are set constant values denoted R and I, respectively, to perform a constant unity gain phase rotation defined by the rotation matrix

$$Q = \begin{bmatrix} R & I \\ -I & R \end{bmatrix}.$$

The angle of rotation is defined to be $\angle Q = -\angle P(j\omega_n)$. The rotation is given unity gain to isolate adjustment of the controller's phase from adjustment of the controller's gain using the gain parameter K. Thus, given a plant frequency response $P(\omega_n) = R_p + jI_p$, R and I are defined to be

$$R = \frac{R_p}{\sqrt{R_p^2 + I_p^2}} \quad \text{and} \quad I = \frac{I_p}{\sqrt{R_p^2 + I_p^2}}$$

Alternatively, dynamic phase compensation uses frequency varying $H_d(s)$ and $H_x(s)$ to dynamically invert the phase of $P(s)$ in a neighborhood around ω_n. It will be shown

dynamic phase compensation increases the gain and phase margin and reduces peaking in the sensitivity function of the closed-loop system when the plant has rapidly changing phase. Dynamic expressions for $H_d(s)$ and $H_x(s)$ will be developed in Section IV.

B. Controller Advantages

A modulated-demodulated controller has been chosen over other repetitive controller architectures primarily because of the decoupling provided between adjacent narrowband control loops. It is possible to target specific frequencies, even those which are not harmonics of the fundamental, for disturbance rejection or reference tracking. It could be useful to track a desired waveform and cancel periodic disturbances at unrelated frequencies. Additionally, independent command of each loop gain provides control over of the convergence rate at frequency. The convergence rate of the controller can be shown to approximately be

$$e^{-\frac{1}{2}\delta_n t}$$

where δ_n denotes the bandwidth of the closed-loop system at frequency ω_n. It is advantageous to adjust the bandwidth of the individual control loops by specifying loop gains inversely proportional to the plant magnitude to avoid excessively different convergence rates. This is important in the pulsed jet application where the magnitude of the frequency response varies by almost two orders of magnitude within our actuation bandwidth.

When digitally implemented, the sampling rate of the modulated-demodulated controller does not have to be an integer multiple of the control frequency. This is an advantage over time delay controllers, which require an integer number of samples in the time delay to generate a sequence with a period exactly corresponding to the fundamental frequency of the disturbance or reference.

IV. CONTROLLER ANALYSIS

As in [10], it is beneficial to analyze the modulated-demodulated controller presented in the previous section from two different perspectives. The first method derives an exact LTI transfer function for the controller from y to u. The second looks at the system from the perspective of the baseband, dividing the system into a two input, two output

(TITO) baseband controller, from $\begin{bmatrix} y_1 & y_2 \end{bmatrix}^T$ to $\begin{bmatrix} u_1 & u_2 \end{bmatrix}^T$ and a TITO compensated plant, from $\begin{bmatrix} u_1 & u_2 \end{bmatrix}^T$ to $\begin{bmatrix} y_1 & y_2 \end{bmatrix}^T$.

A. Control Band Analysis

The fact the controller can be represented as an LTI system is not straightforward. Using Laplace transforms with an arbitrary phase given to the modulating and demodulating signals, $\cos(\omega_n t + \gamma)$ and $\sin(\omega_n t + \gamma)$, it can be shown the transfer function for control at a single frequency is given by

$$C(s) =$$
$$K \left[\frac{H_{LP}(s - j\omega_n)(H_d(s - j\omega_n) - jH_x(s - j\omega_n))}{s - j\omega_n} \right.$$
$$\left. + \frac{H_{LP}(s + j\omega_n)(H_d(s + j\omega_n) + jH_x(s + j\omega_n))}{s + j\omega_n} \right]$$

which is independent of γ and, thus, is time invariant. Using integrators in the baseband has produced the required poles at $\pm j\omega_n$ for perfect steady state tracking of periodic references as dictated by the internal model principle. The poles of $H_{LP}(s)$ have also been shifted to $\pm j\omega_n$, creating a bandpass filter positioned around ω_n with corner frequencies at $\omega_n \pm \omega_c$. It is worth noting that without decoupling ($H_{LP}(s)$=1) and phase compensation ($H_d(s) = 1$ and $H_x(s) = 0$), the modulated and demodulated controller is equivalent to the Internal Model Principle controller $C_{imp}(s)$, which was shown in [9].

It is simple to analyze the stability characteristics of this closed-loop system, $L_n(s) = C_n(s)P(s)$, using Nyquist criterion. However, to gain a better understanding of the phase characteristics of the system and to derive the dynamic expressions for $H_d(s)$ and $H_x(s)$ it is beneficial to study the controller from the baseband perspective.

B. Baseband Analysis

The motivation for development of dynamic phase compensation is best illustrated by baseband analysis of the controller. A compensated plant, $G_n(s)$, is defined as the TITO system from $\begin{bmatrix} u_1 & u_2 \end{bmatrix}^T$ to $\begin{bmatrix} y_1 & y_2 \end{bmatrix}^T$. This is a linear, time-periodic system that can be approximated by an LTI system for frequencies sufficiently close to DC.

The 2×2 system of transfer functions for the compensated plant is given by

$$G_n(s) = \begin{bmatrix} Y_d(s) & Y_x(s) \\ -Y_x(s) & Y_d(s) \end{bmatrix}$$

where

$$Y_d(s) = K\frac{1}{2} \left[P(s - j\omega_n)(H_d(s) + jH_x(s)) \right.$$
$$\left. + P(s + j\omega_n)(H_d(s) - jH_x(s)) \right] H_{LP}(s)$$

$$Y_x(s) = K\frac{j}{2} \left[-P(s - j\omega_n)(H_d(s) + jH_x(s)) \right.$$
$$\left. + P(s + j\omega_n)(H_d(s) - jH_x(s)) \right] H_{LP}(s)$$

Using static phase compensation ($H_d(s) = R$ and $H_x(s) = I$), $Y_x(0) = 0$ provided Q exactly inverts the plant

phase at ω_n. Additionally, $Y_d(0) = 1$ provided both K and Q exactly invert the magnitude and phase of the plant at ω_n, therefore,

$$G_n(0) = I_2.$$

The two branches of the baseband are decoupled at DC. This effectively isolates control of the in-phase and quadrature terms of the demodulated signal. In general, only at $s = 0$ will $G_n(s)$ be diagonal even with $\angle Q = -\angle P(j\omega_n)$. It is likely any physical plant will have changing phase in the neighborhood of ω_n and, therefore, the controller will not exactly invert the plant phase except at ω_n. This has the potential to significantly degrade the performance of the controller, causing peaking in the sensitivity function close to the control frequency.

The use of dynamical compensation instead of static compensation provides the flexibility to diagonalize $G_n(s)$ over a narrow band instead of at $s = 0$ only. The benefit of $G_n(s)$ diagonalization, which is equivalent to inversion of the plant phase in a neighborhood around ω_n, is greatest when the plant has rapidly varying phase around ω_n. It can be shown the diagonal and off-diagonal compensators take the form

$$H_d(s) = \frac{P(s - j\omega_n) + P(s + j\omega_n)}{2P(s - j\omega_n)P(s + j\omega_n)}$$

$$H_x(s) = j\frac{P(s - j\omega_n) - P(s + j\omega_n)}{2P(s - j\omega_n)P(s + j\omega_n)}$$

C. Implementation

In order to implement dynamic phase compensation in our controller, a model fit of the diagonal and off-diagonal compensators must be made using the identified plant data. The models are designed to capture large magnitude and phase changes in the empirical compensators over the widest frequency range possible while retaining accuracy and stability. For example, Figure 4 displays the empirical and fitted phase compensators used for control at 100Hz. The diagonal and off-diagonal empirical compensators have been fit up to a frequency of 40Hz using a 4th order state-space model. The location of the two modes in each compensator have been well captured for both $H_d(s)$ and $H_x(s)$.

D. Single Frequency Example

The improvement provided by dynamic phase compensation over static phase compensation is most clearly illustrated by comparing the stability margins and sensitivity characteristics of each system for control at 100Hz. The Nyquist plot of the static and dynamic phase compensation controller loop gains measured empirically using a gain of 50 is shown in Figure 5. The static phase locus moves closer to encircling -1 than the dynamic phase locus. This has a significant impact on the phase margin of the controller which is 21.6^o for static phase compensation but 60.0^o for dynamic phase compensation.

The phase margin improvement provided by dynamic phase compensation works to reduce peaking in the sensitivity function of the closed-loop system. Figure 6 shows
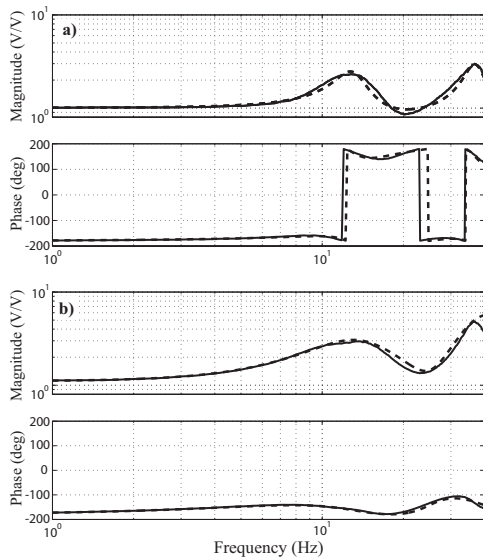
Fig. 4. Dynamic phase compensators for plant phase inversion in a neighborhood around the control frequency. Solid line - empirical, dashed line - model fit. a) $H_d(s)$, b) $H_x(s)$.
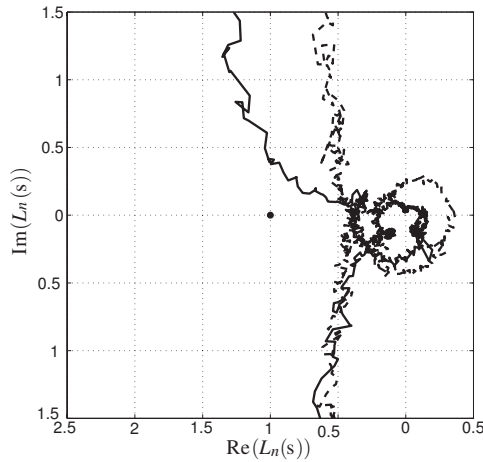

Fig. 5. Nyquist plot comparison of static phase compensation (solid) to dynamic phase compensation (dashed) for control at 100Hz with $K = 50$.

the sensitivity function of the static and dynamic phase compensation systems with $K = 50$. The peak of 3.46 at 92.5Hz is reduced to 1.94 at 81.3Hz and the bandwidth of the system is increased from 10.1Hz to 16.5Hz when dynamic phase compensation is used in place of static phase compensation. Such an improvement is possible due to the rapidly changing plant phase near ω_n, which decreases by 45.4^o, from -86.1^o to -131.5^o, between 92.5Hz and the control frequency at 100Hz.

V. MULTI-FREQUENCY EXPERIMENTAL STUDY

It is fairly commonplace to track or reject sinusoidal references or disturbances at one or two frequencies but for our application the task must be accomplished with a high number of frequencies in order to form a periodic square wave. In the following experiments we use a 20 frequency modulated-demodulated controller with dynamic phase com-
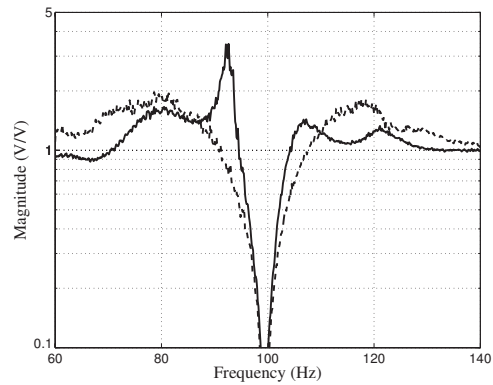

Fig. 6. Sensitivity function comparison of static phase compensation (solid) to dynamic phase compensation (dashed) for control at 100Hz with $K = 50$.

pensation implemented on frequencies [100, 200, 300, 400] Hz. A fundamental frequency of 100Hz is chosen so all 20 frequencies fall within the actuation system bandwidth.

A. Harmonic Rejection

The response of the jet to single or dual tone forcing demonstrates the difficulty open-loop or conventional closed-loop control has in shaping a square wave velocity profile. A single tone input at any frequency produces a jet response at the input frequency as well as a large number of its harmonics. For example, Figure 7a shows perturbations at 200Hz and higher frequencies in response to a single 100Hz input. These harmonics, unaccounted for in open-loop forcing, produce large asymmetries and ringing in the jet's temporal waveform if uncontrolled. The spectrum of the response to the same amplitude input at 100Hz in Figure 7b, this time applied with the closed-loop controller on-line, shows a complete reduction in the harmonic production at nearly all frequencies under control. At each frequency of control the spectrum has been reduced beneath the broadband noise.

Figure 7c shows the spectrum of the response of the system to dual tone inputs at 300Hz and 400Hz with the loop open. Harmonics of each tone appear in the jet response as well as a subharmonic at a frequency equal to the difference between the input tones, 100Hz. A production of subharmonics in this manner is similar to intermodulation distortion. Like the 100Hz single tone case, Figure 7d shows closed-loop forcing of these dual tones eliminates the harmonics as well as the subharmonics.

B. Square Wave Tracking

The reference signal used for square wave forcing is built using the Fourier series coefficients of the square wave. The ideal waveform has a frequency defined by the fundamental forcing frequency but has a variable duty cycle α, the ratio of the temporal pulse width, τ to the waveform period, T, $\alpha = \frac{\tau}{T}$. The duty cycle is varied to pinpoint the forcing conditions which optimize important characteristics of the jet such as penetration or spread. The desired Fourier series coefficients are tracked to produce waveforms such as those shown in Figure 8 with $\alpha = 20\%$ and $\alpha = 40\%$. The
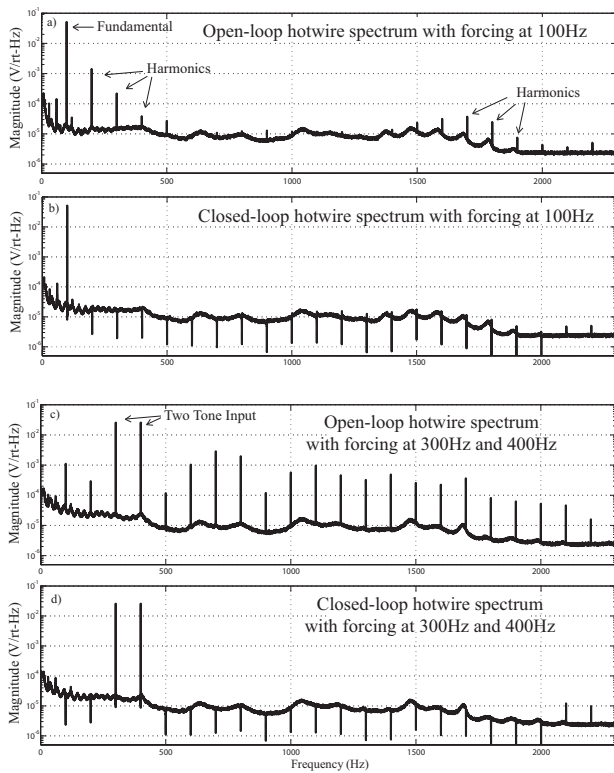
Fig. 7. Suppression of harmonic distortion in response to a 100 Hz single tone input (a) open-loop, b) closed-loop) and elimination of intermodulation distortion in response to a 300Hz and 400Hz dual tone input (c) open-loop, d) closed-loop).
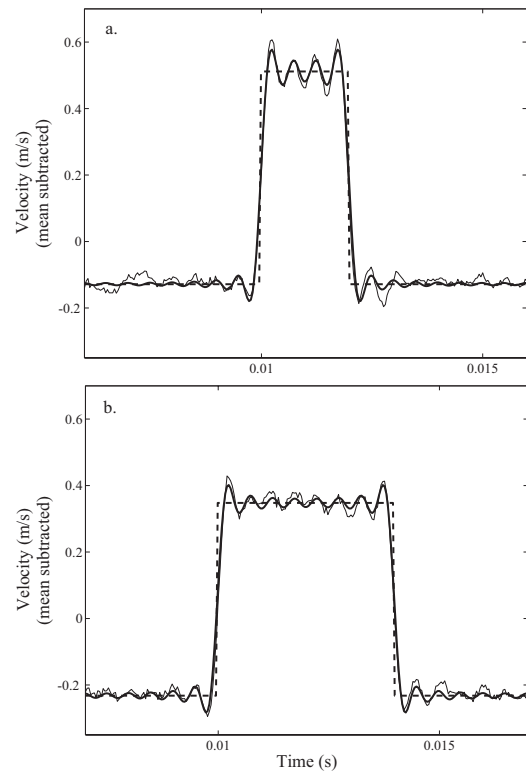

Fig. 8. Square wave with a) $\alpha = 20\%$, b) $\alpha = 40\%$. One period of an ideal square wave (dashed line) is compared to the ideal truncated square wave (thick solid line) and the empirical square wave (thin solid line).

measured waveforms in the thin solid line are compared to the ideal square wave in the dashed line and the truncated Fourier series in the thick solid line. In all cases the measured waveforms match the ideal truncated waveform very well. The small deviations that occur are due to noise which falls outside the narrow band regions around each harmonic and, therefore, is uncompensated.

VI. CONCLUSION

This paper has detailed a useful improvement upon conventional phase compensation of modulated-demodulated control and demonstrated an experimental implementation of such a controller for the application of pulsed jet injection via temporal velocity waveform tracking. The use of dynamic phase compensation instead of constant or static phase compensation has reduced peaking in the sensitivity function and increased the bandwidth of systems for control of plants with varying phase near the disturbance or tracking frequency. It was also shown this controller can be used to simultaneously control a large number of frequencies to track a periodic square wave. The well defined square waves formed in the jet's velocity profile presented in this paper have the potential to significantly improve the spread and mixing of jets used in a variety of aerospace applications.

REFERENCES

[1] T. C. Tsao and M. Tomizuka, "Robust adaptive and repetitive digital tracking control and application to a hydraulic servo for noncircular machining," *Journal of Dynamical Systems, Measurement, and Control*, vol. 116, pp. 24–32, 1994.
[2] S.-C. Wu and M. Tomizuka, "Repeatable runout compensation for hard disk drives using adaptive feedforwad cancellation," *Proc. Amer. Control Conf., MN*, pp. 382–387, 2006.
[3] A. Sacks, M. Bodson, and P. Khosla, "Experimental results of adaptive periodic disturbance cancellation in a high performance magnetic disk drive," *ASME Journal of Dynamical Systems, Measurement, and Control*, vol. 118, pp. 416–424, 1996.
[4] S. Bittanti and L. Moiraghi, "Active control of vibrations in helicopters via pole assignment techniques," *IEEE Transactions on Control Systems Technology*, vol. 2, no. 4, pp. 343–350, 1994.
[5] K. B. Ariyur and M. Krstić, "Feedback attenuation and adaptive cancellation of blade vortex interaction on a helicopter blade element," *IEEE Transactions on Control Systems Technology*, vol. 7, no. 5, pp. 596–605, 1999.
[6] B. A. Francis and W. M. Wonham, "The internal model priciple for linear multivariable regulators," *Applied Mathematics and Optimization*, vol. 12, pp. 457–465, 1975.
[7] T. H. Kandil, H. K. Khalil, J. Vincent, T. L. Grimm, W. Hartung, J. Popielarski, R. C. York, and S. Seshagiri, "Adaptive feedforward cancellation of sinusoidal disturbances in superconducting rf cavities," *Nuclear Intruments and Methods in Physics Research*, vol. 550, pp. 514–520, 2005.
[8] M. F. Byl, S. J. Ludwick, and D. L. Trumper, "A loop shaping perspective for tuning controllers with adaptive feedforward cancellation," *Precision Engineering*, vol. 29, pp. 27–40, 2005.
[9] M. Bodson, A. Sacks, and P. Khosla, "Harmonic generation in adaptive feedforward cancellation schemes," *IEEE Transactions on Automatic Control*, vol. 39, pp. 1939–1944, 1994.
[10] K. Lau, D. E. Quevedo, B. J. G. Vautier, G. C. Goodwin, and S. O. R. Moheimani, "Design of modultated and demodulated controllers for flexible structures," *Control Engineering Practice*, vol. 15, pp. 377–388, 2005.
[11] K. Lau, G. C. Goodwin, and R. T. M'Closkey, "Properties of modulated and demodulated systems with implications to feedback limitations," *Automatica*, vol. 41, pp. 2123–2129, 2005.